# Modulation of the Ganges-Brahmaputra river plume by the Indian Ocean Dipole and Eddies inferred from satellite observations

Severine Fournier, Jérôme Vialard, Matthieu Lengaigne, T. Lee, M. M. Gierach, Akurathi Venkata Sai Chaitanya

AGU PUBLICATIONS

JGR

Journal of Geophysical Research: Oceans

RESEARCH ARTICLE

10.1002/2017JC013333

**Key Points:**
- SMAP provides unprecedented views of the Ganga-Brahmaputra freshwater plume on synoptic to interannual time scales
- The interannual variability of the freshwater plume is modulated by mesoscale eddies and the Indian Ocean Dipole
- SMAP can help improve the understanding and monitoring of salinity impacts on regional climate, tropical cyclones, and oceanic productivity

**Supporting Information:**
- Supporting Information S1

**Correspondence to:**
S. Fournier,
severine.fournier@jpl.nasa.gov

**Citation:**
Fournier, S., Vialard, J., Lengaigne, M., Lee, T., Gierach, M. M., & Chaitanya, A. V. S. (2017). Modulation of the Ganges-Brahmaputra river plume by the Indian Ocean dipole and eddies inferred from satellite observations. *Journal of Geophysical Research: Oceans*, *122*, 9591–9604. https://doi.org/10.1002/2017JC013333

Received 7 AUG 2017
Accepted 9 NOV 2017
Accepted article online 17 NOV 2017
Published online 8 DEC 2017



# Modulation of the Ganges-Brahmaputra River Plume by the Indian Ocean Dipole and Eddies Inferred From Satellite Observations

**S. Fournier[1], J. Vialard[2], M. Lengaigne[2,3], T. Lee[1], M. M. Gierach[1], and A. V. S. Chaitanya[4]**

[1]Jet Propulsion Laboratory, California Institute of Technology, Pasadena, CA, USA, [2]LOCEAN-IPSL, IRD/CNRS/UPMC/MNHN, Sorbonne Universités, Paris, France, [3]Indo-French Cell for Water Sciences, IISc-NIO-IITM-IRD Joint International Laboratory, NIO, Goa, India, [4]National Institute of Oceanography, Council of Scientific & Industrial Research, Goa, India

**Abstract** The Bay of Bengal receives large amounts of freshwater from the Ganga-Brahmaputra (GB) river during the summer monsoon. The resulting upper-ocean freshening influences seasonal rainfall, cyclones, and biological productivity. Sparse in situ observations and previous modeling studies suggest that the East India Coastal Current (EICC) transports these freshwaters southward after the monsoon as an approximately 200 km wide, 2,000 km long "river in the sea" along the East Indian coast. Sea surface salinity (SSS) from the Soil Moisture Active Passive (SMAP) satellite provides unprecedented views of this peculiar feature from intraseasonal to interannual timescales. SMAP SSS has a 0.83 correlation and 0.49 rms-difference to 0–5 m in situ measurements. SMAP and in stu data both indicate a SSS standard deviation of ∼0.7 to 1 away from the coast, that rises to 2 pss within 100 km of the coast, providing a very favorable signal-to-noise ratio in coastal areas. SMAP also captures the strong northern BoB, postmonsoon cross-shore SSS contrasts (∼10 pss) measured along ship transects. SMAP data are also consistent with previous modeling results that suggested a modulation of the EICC/GB plume southward extent by the Indian Ocean Dipole (IOD). Remote forcing associated with the negative Indian Ocean Dipole in the fall of 2016 indeed caused a stronger EICC and "river in the sea" that extended by approximately 800 km further south than that in 2015 (positive IOD year). The combination of SMAP and altimeter data shows eddies stirring the freshwater plume away from the coast.

**Plain Language Summary** The Bay of Bengal receives large quantity of freshwater from the Ganges-Brahmaputra river during the monsoon. The resulting low-salinity sea surface has strong implications for the regional climate and living marine resources. In situ observations are too sparse to provide salinity maps in this basin, even every 3 months. In contrast, the SMAP satellite provides maps at 40 km resolution, every 8 days, opening great perspectives for studying salinity in the Bay of Bengal. In this article, we show that SMAP compares well with in situ data, even close to the coast. The Ganges Brahmaputra freshwater plume is transported over 2000 km by the East Indian Coastal Current. We further show that climate variability and mesoscale variability induce strong year-to-year variations in the way this freshwater plume expands along the east coast of India.

## 1. Introduction

Monsoonal rains feed several powerful rivers that flow into the Bay of Bengal (BoB), with largest discharge during and shortly after the southwest monsoon. The Ganga-Brahmaputra (GB) River located in the very northern end of the BoB is the largest by far, accounting for two-thirds of the total river discharge into the BoB (1,300 $km^3$ climatologically during June–September) (Dai & Trenberth, 2002; Papa et al., 2012). Oceanic rainfall also contributes in equal proportion to the total freshwater received by the northern BoB (Chaitanya et al., 2014). Consequently, the BoB stands out as the freshest marginal sea in the tropics (Chaitanya et al., 2014), with SSS being as low as 25 pss (Wijesekera et al., 2016) and displaying sharp horizontal gradients (Sengupta et al., 2016).

These low SSS can impact air-sea interactions in the BoB by maintaining a thin mixed layer and favoring the formation of an isothermal salinity-stratified layer between the surface mixed layer and colder thermocline

water, known as the barrier layer (Rao & Sivakumar, 2003; Vinaychandran et al., 2002). This strong salinity stratification inhibits vertical mixing between the surface mixed layer and subsurface colder, nutrient-rich water (Thadathil et al., 2016; Vialard & Delecluse, 1998). This maintains high climatological surface temperatures, above the 28°C threshold necessary for deep atmospheric convection, contributing to the climatologically strong rainfall during the southwest monsoon (Shenoi et al., 2002). This also limits cooling below tropical cyclones (Neetu et al., 2012; Sengupta et al., 2008), which can favor their intensification (Cione & Uhlhorn, 2003). Finally, the strong salinity stratification could be one of the reasons for the rather low BoB biological productivity compared to the Arabian Sea (Prasanna Kumar et al., 2002). Previous studies have shown that there is a strong seasonal (Akhil et al., 2014) and interannual (Akhil et al., 2016b; Chaitanya et al., 2015) SSS variability in the BoB. It is hence necessary to better monitor the BoB SSS, in order to improve the understanding of salinity impacts on regional climate, tropical cyclones, and biological productivity.

Ocean currents play a prominent role in the BoB SSS space-time variations. In particular, the BoB hosts a western boundary current known as the East Indian Coastal Current (EICC). The EICC reverses seasonally (Yu et al., 1991) in response to the combined influence of local BoB and remote equatorial monsoonal winds (McCreary et al., 1996). It flows southward with a speed of approximately 0.5 m $s^{-1}$ during the October–December period (Durand et al., 2009) due to the combined effect of northeasterlies associated with the winter monsoon and remote forcing from intermonsoon equatorial westerlies (McCreary et al., 1996). The EICC is confined to the western boundary, with a narrow climatological width of less than 50 km north of 10°N, although frequent occurrence of eddies in this region often induces wider ∼150–200 km recirculating loops (Durand et al., 2009).

The EICC flows past the GB River mouth. This is expected to transport the GB-induced freshwater southward along the east coast of India (Chaitanya et al., 2014). Shetye et al. (1996) documented such a narrow coastal freshwater plume southwest of the GB mouth based on in situ observations collected during a cruise in December 1991, with an 8 pss drop over 100 km toward offshore at 12°N near the Indian coast. Hareesh Kumar et al. (2013) also used in situ measurements to highlight a strong thermohaline front off the east coast of India in December 1997, with an offshore meandering due to mesoscale eddies. Recently, Chaitanya et al. (2014) used in situ observations collected by fishermen along the east coast of India to demonstrate that this ∼200 km wide freshwater tongue (referred to as a "river in the sea") is a seasonally recurring feature, whose expansion is coincidental with the development of the southward-flowing EICC. The modeling study by Akhil et al. (2014) confirmed that the "river in the sea" expands southward due to advection of low salinities from the GB outflow region by the EICC, while its decay is due to erosion through vertical mixing.

In addition to seasonal variations, the BoB climate also exhibits strong precipitation and runoff interannual variations (Papa et al., 2012). This led Akhil et al. (2016b) to investigate the causes of the SSS interannual variability in the BoB. They found that interannual variations in GB runoff only contribute to interannual SSS variations locally near the river mouth in the northern BoB. In contrast, the southward expansion of the "river in the sea" is strongly influenced by circulation changes associated with the Indian Ocean Dipole (IOD). The IOD arises from air-sea interactions in the tropical Indian Ocean, peaks in fall and typically lasts for about 6 months. A positive IOD is associated with anomalous easterly equatorial winds (opposite for negative IOD) that force equatorial upwelling Kelvin waves. Upon reaching the eastern equatorial Indian Ocean, some of this wave energy propagates into the BoB as coastal upwelling Kelvin waves, inducing a negative sea level anomaly (SLA) along the rim of the bay in fall, and an anomalously weak EICC during fall and winter months (Jensen, 2007; Shankar, 1998; Subrahmanyam et al., 2011). Akhil et al. (2016b) showed that this weak EICC transports less water from the GB outflow toward the south, resulting in a weaker southward expansion of the "river in the sea" and a positive SSS anomaly along the coast of India.

Despite the increasing amount of in situ observations, they are still too sparse to provide a systematic and routine monitoring of the spatiotemporal variability of this ∼200 km wide "river in the sea" (Chaitanya et al., 2014) and more generally of the BoB SSS variability, even at the seasonal scale (Figure 1a). Spaceborne SSS observations from recent satellite missions are unique opportunities to significantly enhance these capabilities. These missions include the European Space Agency (ESA) Soil Moisture and Ocean Salinity (SMOS) (Mecklenburg et al., 2012) and National Aeronautics and Space Administration (NASA) Aquarius/Sac-D missions (Lagerloef et al., 2008) launched in 2009 and 2011, respectively. SMOS has a 33 km spatial resolution that is in principle sufficient to monitor this "river in the sea." Unfortunately, while SMOS SSS data are

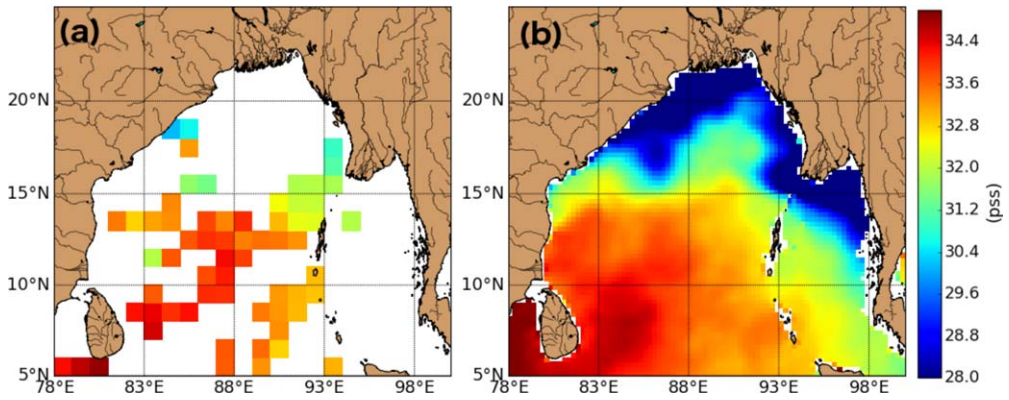


**Figure 1.** (a) September–November 2015 in situ SSS measurements averaged within 1° pixels and (b) September–November 2015 average map of SMAP SSS.

amenable for open ocean applications, the current SMOS SSS retrievals are of poor quality in the BoB due to significant contamination by Radio Frequency Interference (RFI) and land signals (Akhil et al., 2016a; Boutin et al., 2012; Subrahmanyam et al., 2013). In comparison, Aquarius performs much better for monitoring large-scale SSS patterns in the BoB (Akhil et al., 2016a), but is however not suitable to monitor the GB freshwater plume due to its lower (∼110 km) spatial resolution and because measurements within 150 km of the coast are usually contaminated by land signals (Aquarius User Guide, 2015). The Aquarius mission also ended in June 2015 due to a power failure of the SAC-D spacecraft carrying the Aquarius sensor.

Launched on 31 January 2015, NASA's Soil Moisture Active Passive (SMAP) satellite provides SSS observations at a similar spatial resolution to SMOS (40 km) but with a better SSS retrieval close to the coast as it is less sensitive to RFI than SMOS (Reul et al., 2013). Fournier et al. (2016) indeed demonstrated that SMAP SSS compares better to in situ data than SMOS in the Gulf of Mexico (a runoff-impacted marginal sea), especially in coastal areas. SMAP thus has the potential to provide the first synoptic views of the "river in the sea" at the scale of the BoB, and to monitor its seasonal and interannual variations.

Figure 1a shows that in situ data collected in the top 5 m of the BoB over a representative 3 months period (September–November 2015), cover only a small fraction of the BoB. The average SSS from SMAP during the same period is shown in Figure 1b. SMAP has complete coverage of the global ocean every 8 days, an interval over which the coverage by in situ data is even more sparse than that shown in Figure 1a. Therefore, SMAP has much better spatiotemporal coverages than in situ observations. Previous studies of the "river in the sea" either used models, or in situ data with this very limited spatiotemporal coverage. Here, we will characterize its spatial and temporal variations from satellite SSS data for the first time. We will in

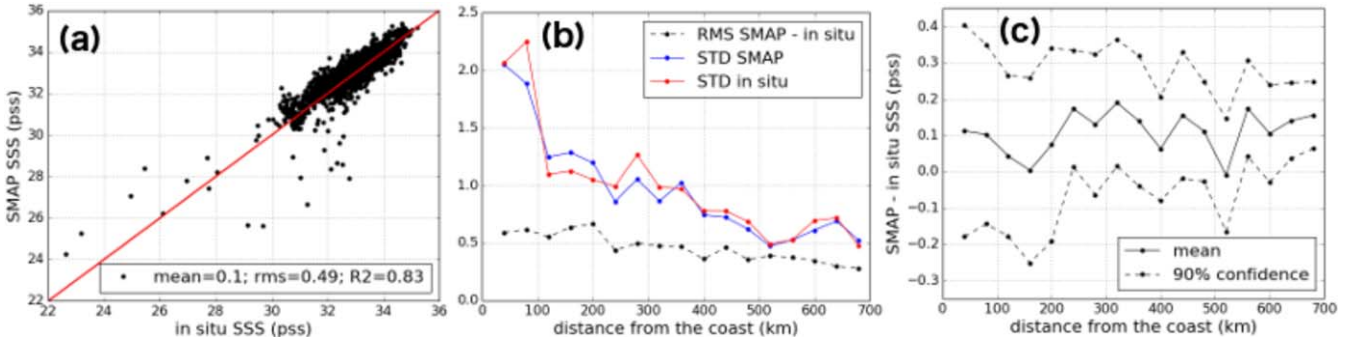


**Figure 2.** (a) April 2015 to December 2016 SMAP versus in situ SSS for the entire BoB. (b) April 2015 to December 2016 SMAP (blue) and in situ (red) SSS standard deviation and RMS of the differences between SMAP and in situ SSS (black) as a function of the distance from the coast (per bin of 40 km), for the entire BoB. For each pixel of the BoB, we compute the distance from the coast as the distance between the pixel and the closest coast of the BoB. (c) April 2015 to December 2016 mean SMAP-in situ SSS differences (continuous line) as a function of the distance from the coast (40 km bins), for the entire BoB. The black-dotted lines show the 90% confidence interval for the SMAP minus in situ SSS differences.

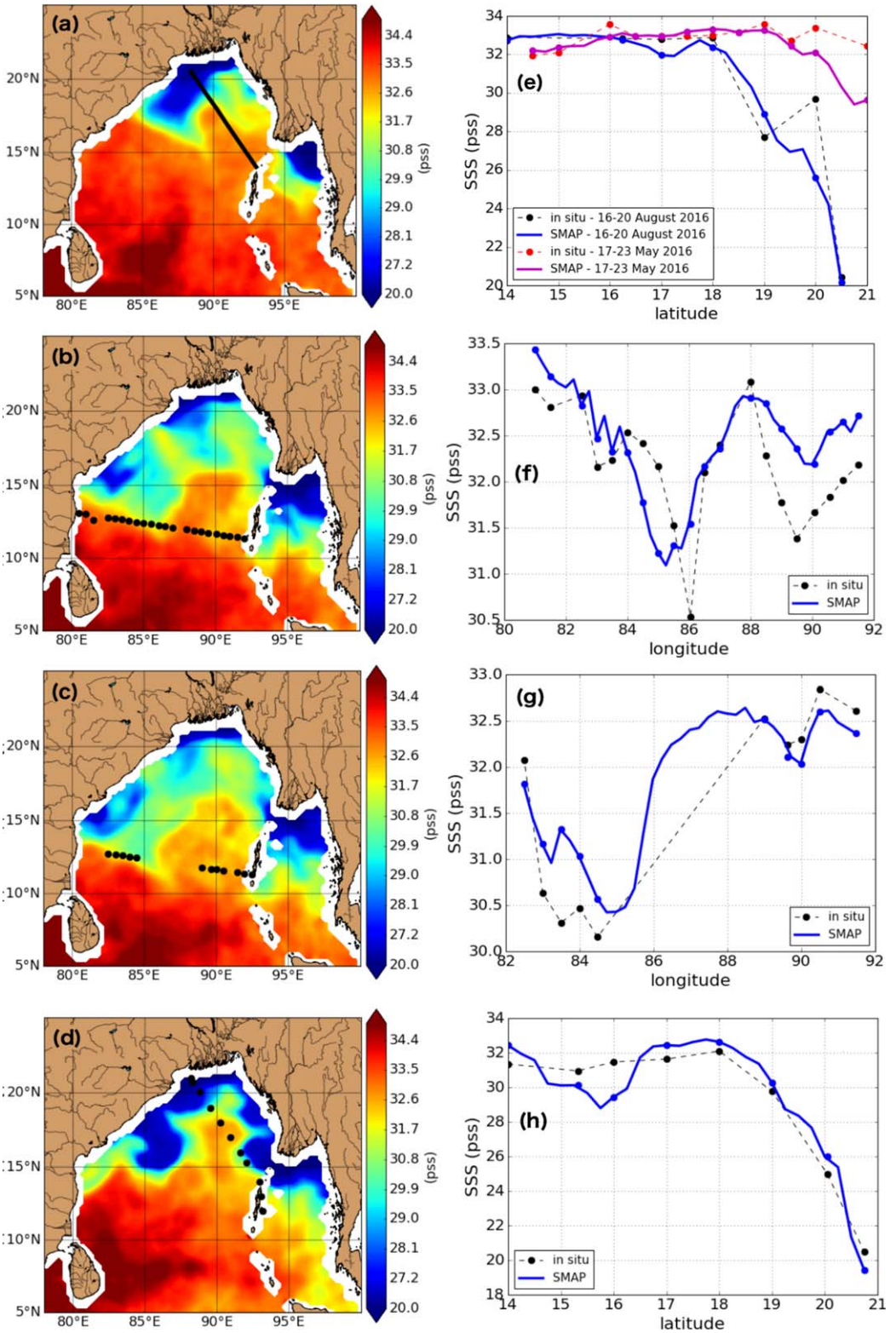


**Figure 3.** (continued)

particular verify the influence of IOD-driven EICC anomalies or eddies on the variability of the plume, proposed by previous modeling studies. The present study is the first demonstration of the capability of satellite SSS to monitor the spatial and temporal distribution of low salinity surface waters in coastal regions of the BoB, which is an essential step to improve our understanding of their impacts on the regional climate, tropical cyclones, and biological productivity.

## 2. Data and Methods

Our analysis is carried out using satellite and in situ measurements, which are briefly described below. All these data sets were averaged to produce monthly values.

We used the Level-3 SMAP SSS version-3 data set produced by the Jet Propulsion Laboratory (Yueh et al., 2013, 2014) at 0.25° horizontal resolution and 8 day running average time window from 31 March 2015 to 31 December 2016. Using SSS retrieval by Remote Sensing Systems (REMSS) yields very similar results (not shown). The horizontal resolution of SMAP SSS is 40 km. However, the data within 40 km of the coasts are often heavily contaminated by land signals due to leakage of signals from the sidelobes of the satellite antenna into the main lobe. Therefore, SMAP data within 40 km of the coasts are excluded. The "river in the sea" hugging the east coast of India has a typical width of 200 km. In the following, we will refer oceanic regions from 40 to 200 km of the coast as coastal regions.

In situ salinity measurements from the World Ocean Database (WOD) over the BoB from April 2015 to December 2016 were extracted using the WOD select tool (https://www.nodc.noaa.gov/OC5/SELECT/dbsearch/dbsearch.html) for validating the satellite SSS. This includes all the data included in the WOD13 product (Boyer et al., 2013), as well as more recent data (largely from Argo profilers) with limited quality control. We only considered data further than 40 km from the coast, where SMAP SSS data are available. Satellite SSS measures the salinity in the top centimeter of the ocean while in situ salinity measurements are typically deeper than 1 m. We used all in situ measurements from the WOD located in the 1–5 m depth range. The implications of the difference in sampling depth between satellite and in situ measurements are discussed in the next section.

We also used in situ data at about 1 m depth from bucket samples collected by the National Institute of Oceanography (Goa, India) on an approximately bimonthly basis along two repeated merchant ship tracks between the Andaman Islands in the southeast Bay of Bengal and Kolkata (near the GB River mouth) and Chennai (at about 12°N along the Indian coast; Chaitanya et al., 2015). The relatively high spatial sampling of this data set allows resolving the strong SSS gradients across the "river in the sea."

We used the Ssalto/Duacs SLA and near-surface ocean current estimates from AVISO to highlight the influence of the regional ocean circulation on SSS variability. Comparisons with in situ data and specifically processed along track altimeter data suggest that this product captures the EICC seasonal variations as close as ∼40 km away from the coast (Durand et al., 2008; their figure 3). The Level-3 SLA and Level-4 geostrophic velocities products are obtained from multisatellite observations at daily interval on a 1/4° × 1/4° grid, from 1993 to present. To better highlight interannual and shorter time scales, the nonnegligible linear trend observed in the Northern Indian Ocean over the 1993–2016 period (Thompson et al., 2016) has been removed.

**Figure 3.** (a)–(d) SMAP SSS on the first day of the transects represented in (e)–(h), respectively, on the (a) 16 August 2016 (first day of the transect showed in blue on plot e), (b) 14 October 2016, (c) 20 October 2016, and (d) 22 October 2015. The black dots represent the in situ measurement locations. (e) SMAP (continuous line) and in situ SSS (dashed line) along the Kolkata-Port Blair transect for the 17–23 May 2016 (magenta for SMAP and red for in situ) and 16–20 August 2016 (blue for SMAP and black for in situ). In situ (black dots connected by dashed lines) and colocated SMAP SSS (blue dots) along each transect as a function of (f) longitude from 14 to 17 October 2016, (g) longitude from 20 to 22 October 2016, and (h) latitude from 22 to 25 October 2015. The SMAP SSS along each transect (one value every ∼40 km) is represented in blue. An offset of 4.4 pss has been applied to in situ data in Figure 3h to correct a calibration problem on the salinometer. Regardless of the causes for the time-mean difference between SMAP and the (in situ) transect data (e.g., calibration issue for the water samples), the spatial variation of the transect data are still useful to evaluate SMAP data. This is the point we are emphasizing in Figure 3h when we remove the time-mean offset in comparing SMAP and the transect data.

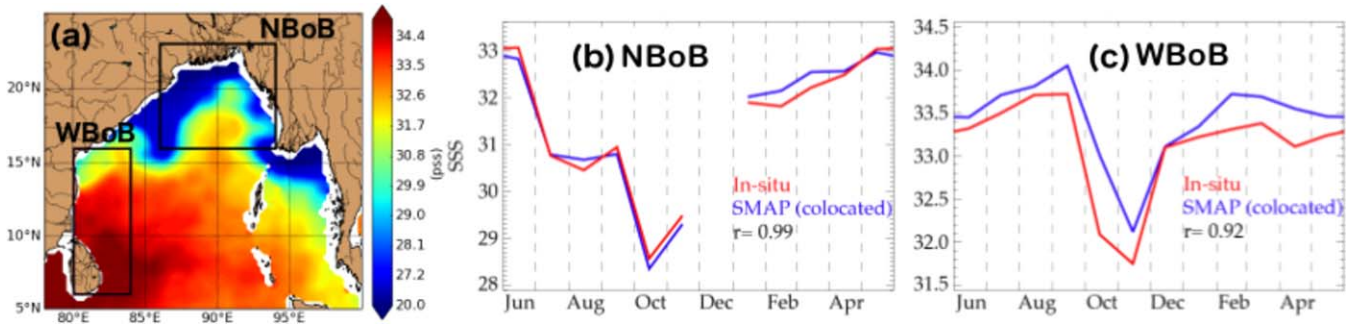


**Figure 4.** (a) Monthly map of SMAP SSS for October 2015. (b) Northern and (c) Western Bay of Bengal (see plot Figure 4a) mean seasonal SSS cycle (computed over April 2015 to December 2016) of available in situ (red) and collocated SMAP (blue) data.

The Dipole Mode Index (DMI) defined by Saji et al. (1999) is an indicator of the anomalous east-west temperature gradient across the tropical Indian Ocean, which reflects the IOD variability. In this study, we used the average September–October–November (SON) DMI provided by the Japan Agency for Marine-Earth Science and Technology (JAMSTEC) (http://www.jamstec.go.jp/frcgc/research/d1/iod/HTML/Dipole%20Mode%20Index.html). The SON DMI has been detrended over 1993–2016 and then normalized. We compute a lead-lag regression of the monthly SLA to the normalized SON DMI, $\eta_{IOD}$. For each year, the monthly SLA signal can then be partitioned into:

$$\eta(x, y, yr, month) = \eta_{SC}(x, y, yr, month) + \mathrm{DMI}_{SON}(yr) * \eta_{IOD}(x, y, yr, month) + \eta_{RES}(x, y, yr, month),$$

where $\eta_{SC}$ represents the mean seasonal cycle, the second term the IOD signal, and $\eta_{RES}$ the residual, which largely reflects mesoscale oceanic eddy variability. The same approach is used for current signals.

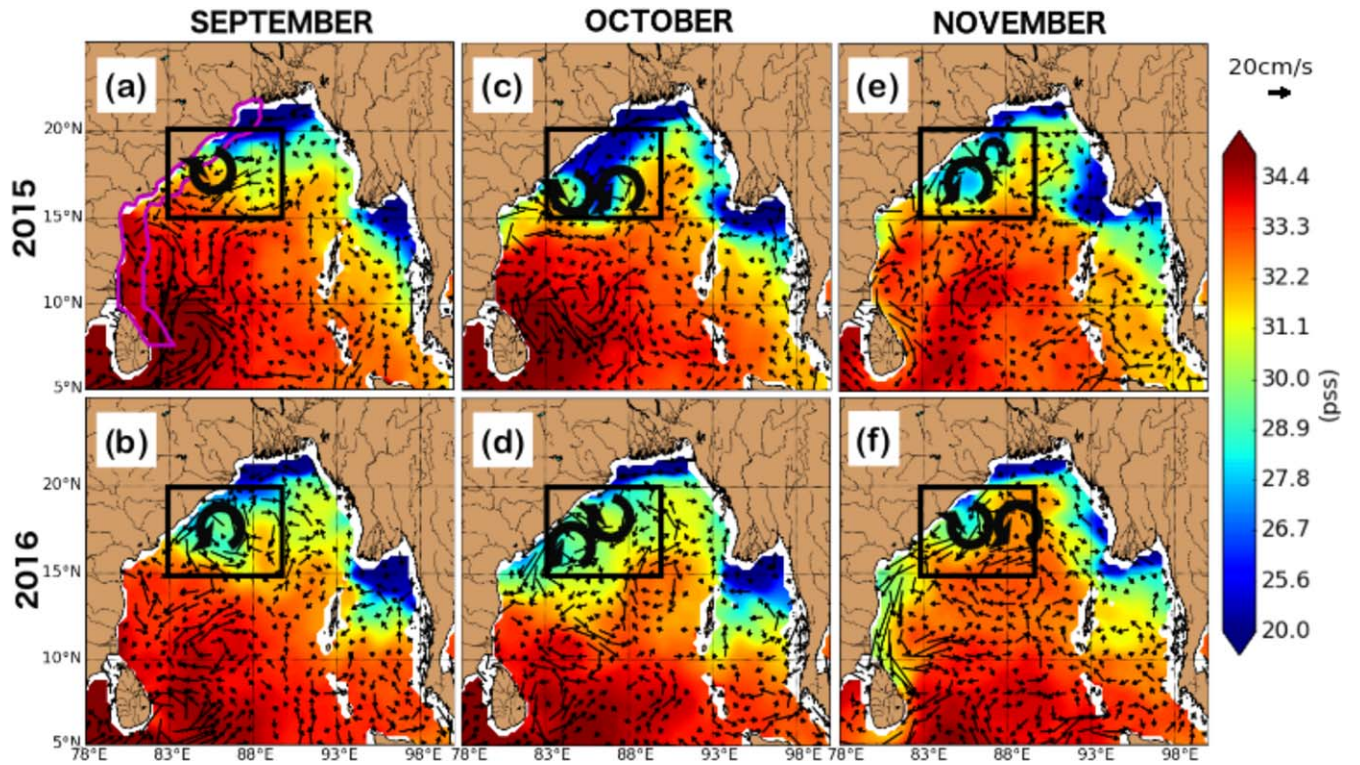


**Figure 5.** (a), (c), and (e) SMAP SSS for September, October, and November in 2015 and (b), (d), and (f) 2016. Monthly AVISO currents are represented on top, only one vector in three is represented and currents below 10 cm $s^{-1}$ are not displayed. Thick arrows highlight eddies which are discussed in the text. The frames outline the zooms shown on Figure 11.

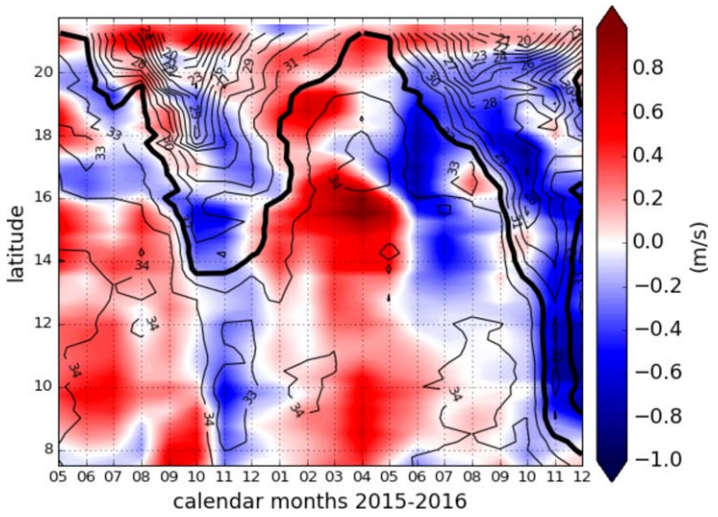


**Figure 6.** May 2015 to December 2016 latitude-time sections of average monthly alongshore currents within 200 km of the East Indian coast (region delimited by a magenta contour on Figure 5a). The average SSS are represented as contours (contour interval: 1 pss; bold 32 pss contour). Currents are shown as positive when they flow toward the North of the bay.

## 3. Results

Figure 2a provides a scatterplot between SMAP and available in situ SSS data from April 2015 to December 2016. SMAP is on average 0.1 pss saltier than the colocated in situ measurements, with a root-mean-squared difference (RMSD) of 0.49 pss and a correlation of 0.83. Figure 2b shows this RMSD as a function of the distance from the coast. The RMSD values within 200 km of the coast (approximately 0.6 pss) are slightly larger than those further offshore (approximately 0.4 pss). These values are much smaller than the standard deviation (i.e., amplitude) of the SSS signals derived from either SMAP or in situ data. Therefore, the SMAP SSS have good signal-to-noise ratio. Similarly, the approximately 0.1 pss bias of SMAP SSS relative to the in situ data does not increase within 200 km of the coast (Figure 2c). Figure 2 is meant to validate the SMAP SSS data in the whole Bay of Bengal for completeness. More specific comparisons of SMAP SSS with in situ data along specific transects that intersect the "river in the sea" in the east coast are presented in Figure 3. The comparisons in Figure 2 suggest that SMAP SSS are accurate enough to monitor the large salinity signals within 100–200 km of the coast in the BoB.

Despite this good overall agreement, SMAP SSS can display large fresh biases (up to 4 pss) for a couple of points in the lower salinity range. These large differences may arise from the very strong near-surface stratification often found in the BoB (i.e., the satellite represents the top millimeter while we use in situ data within 1–5 m depth; Akhil et al., 2016a). A reviewer also pointed out that a potential cause for the saltier Argo salinity measurements in the upper 5 m is Argo CTD mixing near-surface (shallower than 5 m) waters with waters from 4 to 5 m depth, which might be the depth when Argo floats shut off the pumping.

In addition to this, the spatiotemporal sampling differences between satellite SSS (averaged within satellite footprint at 8 day intervals) and point-wise instantaneous in situ measurements can result in substantial RMSD between satellite and in situ SSS in regions with strong horizontal gradients and eddy variability (Boutin et al., 2015), as the northern BoB (Figure 1b). Potential contamination by land signals may also contribute to the fresh biases of SMAP SSS relative to in situ measurements.

We now evaluate SMAP SSS through comparisons with in situ salinity from two transects between the Andaman Islands and Kolkata, near the GB estuary (Figures 3a and 3e). In May 2016, before the southwest monsoon onset, SMAP and in situ measurements display relatively homogeneous SSS around 32–33 pss, except very close to the GB estuary, where SSS drops to ∼30 pss in SMAP. In August 2016 (i.e., after the monsoon onset), SMAP SSS reveals the GB plume spatial extension (with salinities below 28 pss, Figure 3a). In situ data along the transect sample the strong salinity contrast between the GB freshwater plume and saltier interior BoB water. SSS starts decreasing from about 33 pss at 18°N to ∼20 pss (a 13 pss drop) 40 km offshore of the GB estuary (Figure 3e). SMAP SSS retrievals capture this SSS decrease relatively well, except

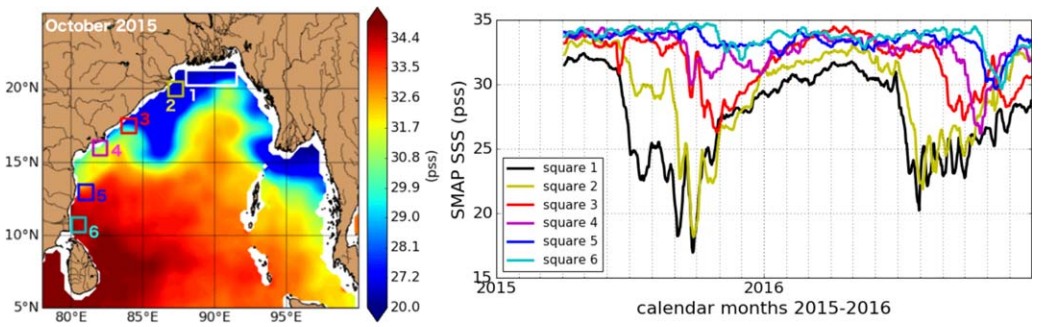


**Figure 7.** (a) Monthly map of SMAP SSS for October 2015. (b) Time series (8 day resolution) of SMAP SSS within the six boxes along the western Bay of Bengal, (see plot Figure 7a) from April 2015 to January 2017.

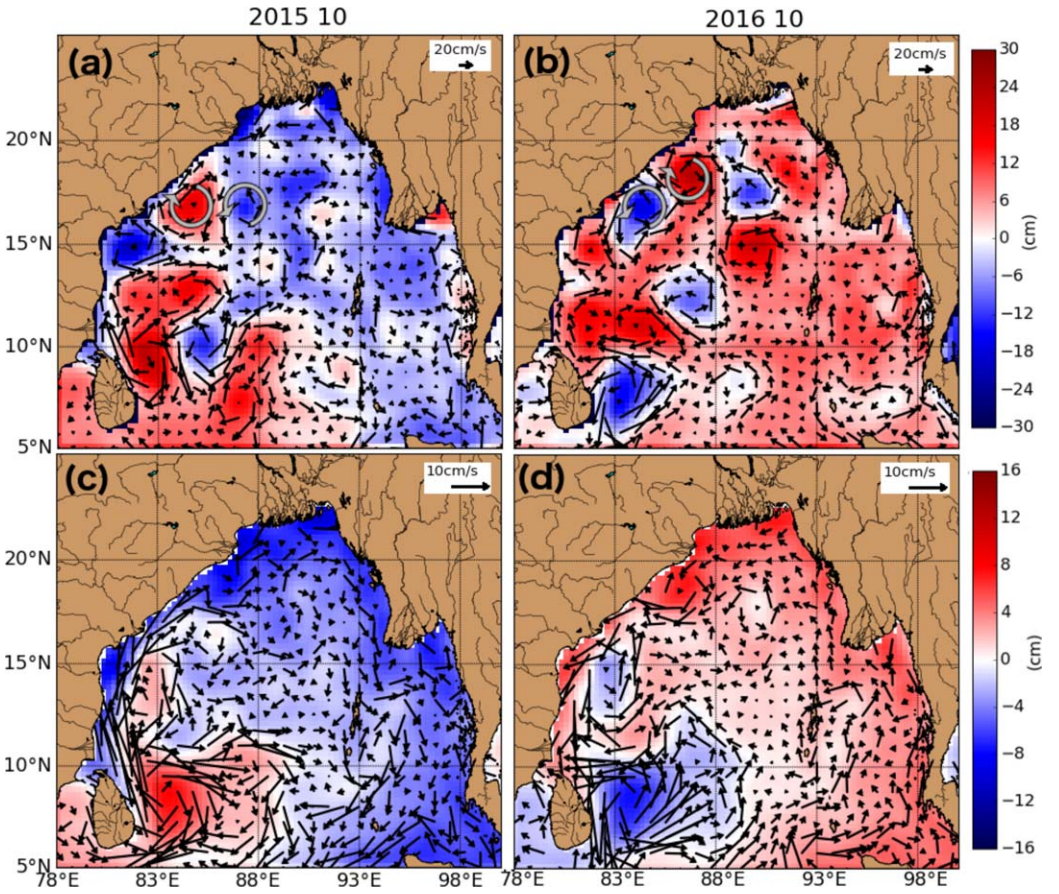


**Figure 8.** (a and b) Monthly maps of SLA and currents anomalies from the climatology in October 2015 and (b) 2016. (c) Monthly maps of SLA and current vectors anomalies with respect to the seasonal cycle associated with the IOD in October 2015 and (d) 2016. Those are obtained through a regression of the aforementioned fields to the normalized SON DMI (Dipole Mode Index). Only one vector in three is represented in all the maps. SLA has been detrended over the period 1993–2016. Thick arrows highlight eddies which are discussed in the text.

at one point near 20°N, close to a large horizontal gradient (Figure 3a). Figure 3 also provides comparisons along three additional selected transects that cross sharp SSS gradients. SMAP retrievals capture the general shape of salinity variations along these transects, including those relatively close (within ∼50–200 km) to the coast and those fresher than 28 pss. Finally, we constructed a mean SSS seasonal cycle from all the available in situ data within two regions selected for their strong SSS variations, i.e., the northern and western BoB (see frames on Figure 4a for the definition of each box), and compared it to the collocated SMAP data (Figures 4b and 4c). The excellent comparison between in situ and collocated SMAP data (correlations $> 0.9$) shows that SMAP captures the large-scale signals in those two boxes. The largest freshening in the northern box occurs in October, and reaches the western box one month later in November, consistent with the results of Chaitanya et al. (2014). However, the short data set duration and poor in situ sampling in these regions imply that the time series shown on Figure 4b,c may not be representative of the long-term SSS seasonal cycle in those boxes.

We now focus on the September–November period, that follows the GB River peak discharge (Papa et al., 2012), to document the southward extension of the "river in the sea" in 2015–2016. Monthly maps of satellite SSS and surface currents for 2015–2016 are provided in Figure 5. In September of both years, the EICC has not yet developed and the GB plume remains confined to the northern BoB (Figures 5a and 5b). The development of the southward-flowing EICC starts transporting this fresh plume southward to ∼15°N in October (Figures 5c and 5d). The "river in the sea" extends further south in November 2016, with SSS below 31 pss reaching Sri Lanka in association with an EICC flowing southward at 0.7 m $s^{-1}$ (Figure 5f). In contrast, it remains confined north of 13°N in November 2015 in association with a far weaker southward-flowing

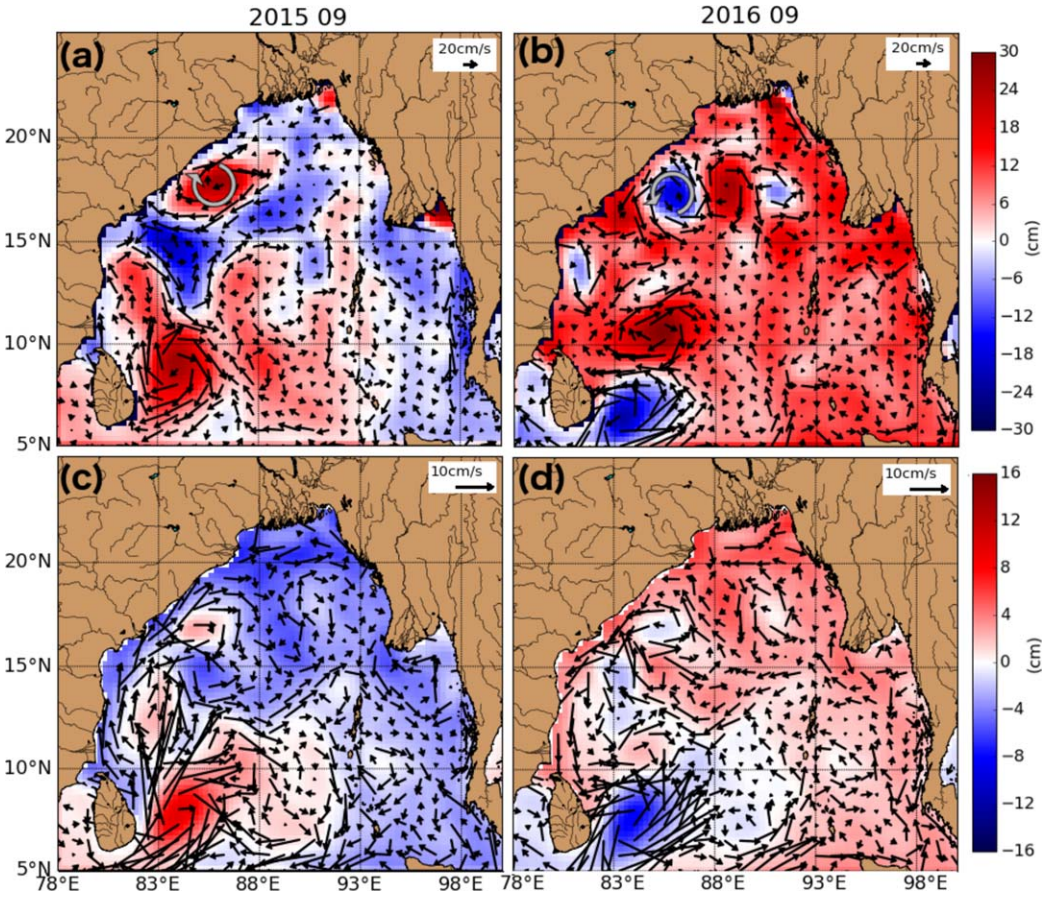


**Figure 9.** (a and b) Monthly SLA and currents anomalies from the climatology in September (a) 2015 and (b) 2016. (c and d) Monthly SLA and current vectors anomalies with respect to the seasonal cycle, associated with the IOD in September (c) 2015 and (d) 2016. Those are obtained through a regression of the aforementioned fields to the normalized SON DMI (Dipole Mode Index). Only one vector in three is represented in all the maps. SLA has been detrended over the 1993–2016 period Thick arrows highlight eddies which are discussed in the text.

EICC (Figure 5e). This difference between the 2015 and 2016 in terms of the southward expansion of the "river in the sea" is confirmed by Figure 6, which shows a latitude-time section of alongshore currents (colors) and SSS (contours) within 200 km of the eastern coast of India (within the magenta contour on Figure 5a). The GB freshwater plume (highlighted by the bold 32 pss contour) clearly extends further south in 2016 than in 2015, reaching 8°N in December 2016 against only 13.5°N in November 2015. Similarly, the southward alongshore surface currents are stronger in 2016 (0.6–0.7 m $s^{-1}$) than they are in 2015 (0.2–0.3 m $s^{-1}$), especially south of 14°N. Figure 7 shows time series of SMAP SSS in several boxes along the east Indian shelf, wherein the freshening southward progression is clearly more visible in the fall of 2016 (SSS is 2–3 pss lower at 16°, 14°, and 11°N).

Based on model results, Akhil et al. (2016b) suggested that the IOD-related wind anomalies remotely control the SSS interannual variations along the east coast of India. Positive IOD events induce easterly equatorial wind anomalies and anticyclonic anomalies in the BoB. These wind anomalies force coastal upwelling Kelvin waves that propagate anticlockwise around the BoB rim. The induced negative sea level anomalies along the eastern coast of India weaken the EICC, hence limiting the southward transport of freshwater. Here we investigate this further using observations. Figures 8a and 8b illustrate the differences in SLA and current anomalies (relative to the mean seasonal cycle) in October 2015 and 2016. While positive SLA anomalies are prominent in most of the BoB in October 2016, negative SLA anomalies dominate in October 2015. The SON DMI detrended and normalized value is +0.97 in 2015 and −0.99 in 2016, i.e., 2015 is a moderate positive IOD event while 2016 is a negative one (opposite IOD polarities are often found in alternate years due to the strong biennial IOD tendency, Saji et al., 1999). Figures 8c and 8d further provide the SLA and current

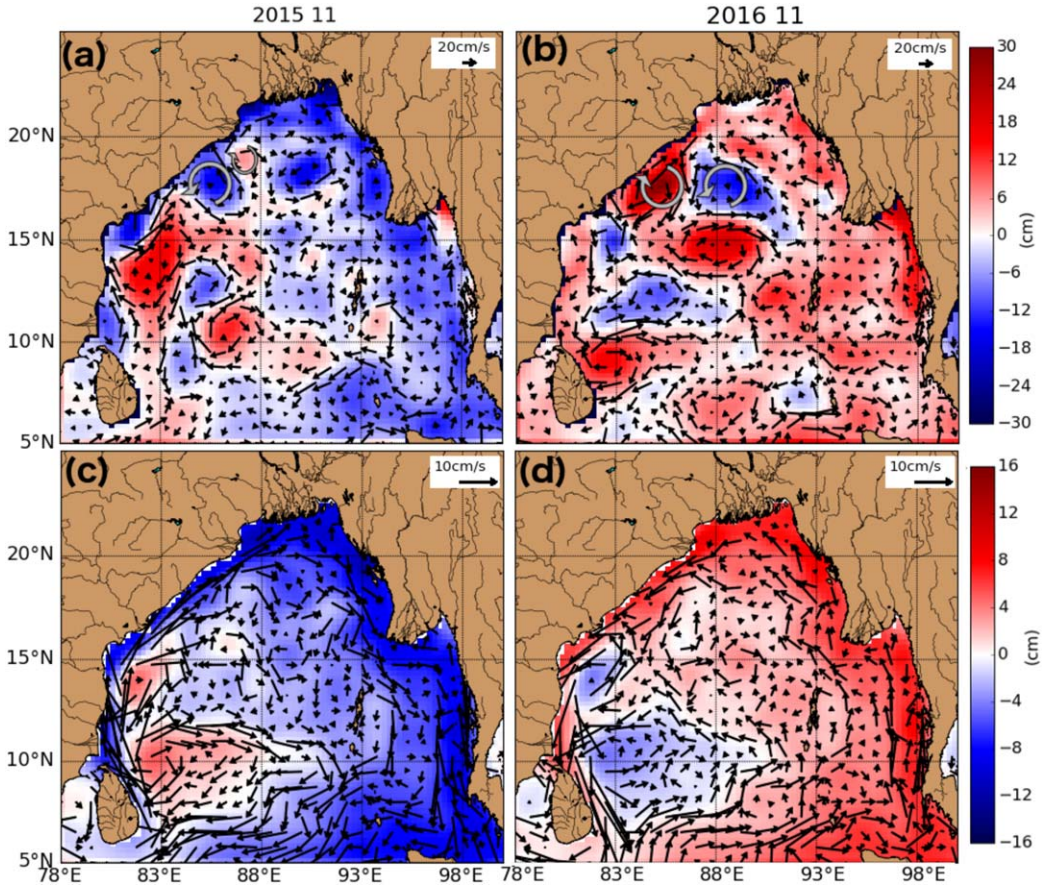


**Figure 10.** (a and b) Monthly SLA and currents anomalies from the climatology in November (a) 2015 and (b) 2016. (c and d) Monthly SLA and current vectors anomalies with respect to the seasonal cycle associated with the IOD in November (c) 2015 and (d) 2016. Those are obtained through a regression of the aforementioned fields to the normalized SON DMI (Dipole Mode Index). Only one vector in three is represented in all the maps. SLA has been detrended over the 1993–2016 period. Thick arrows highlight eddies which are discussed in the text.

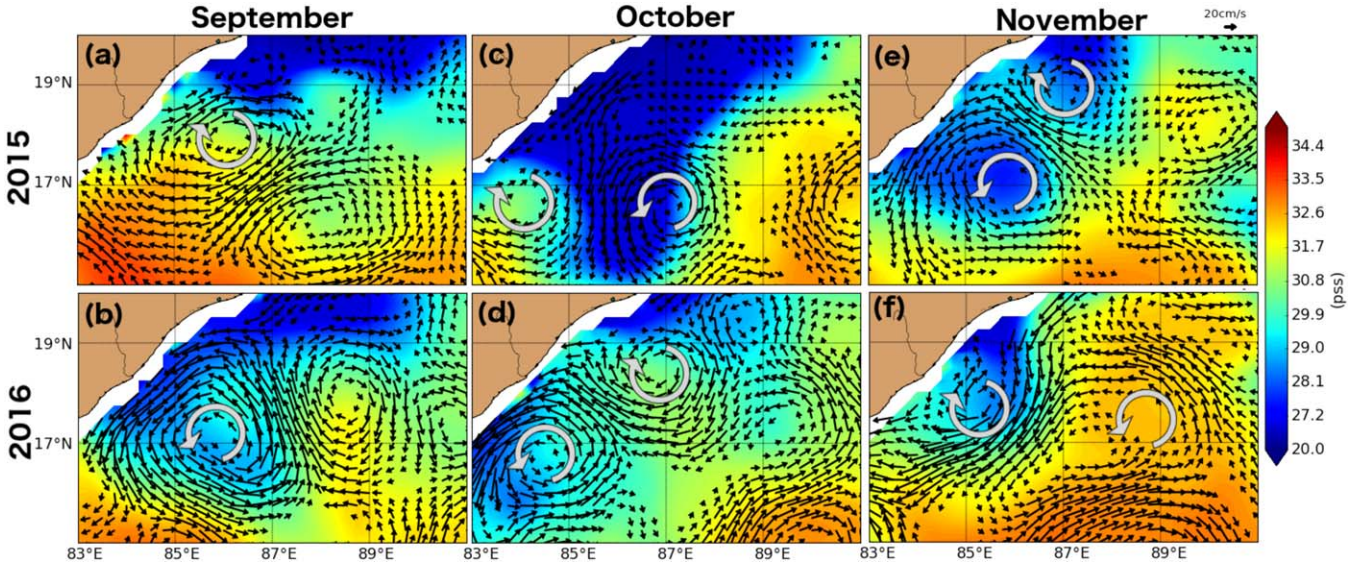


**Figure 11.** Zoom into the frames shown on Figure 5. All current vectors are shown on this plot except currents below 10 cm $s^{-1}$.

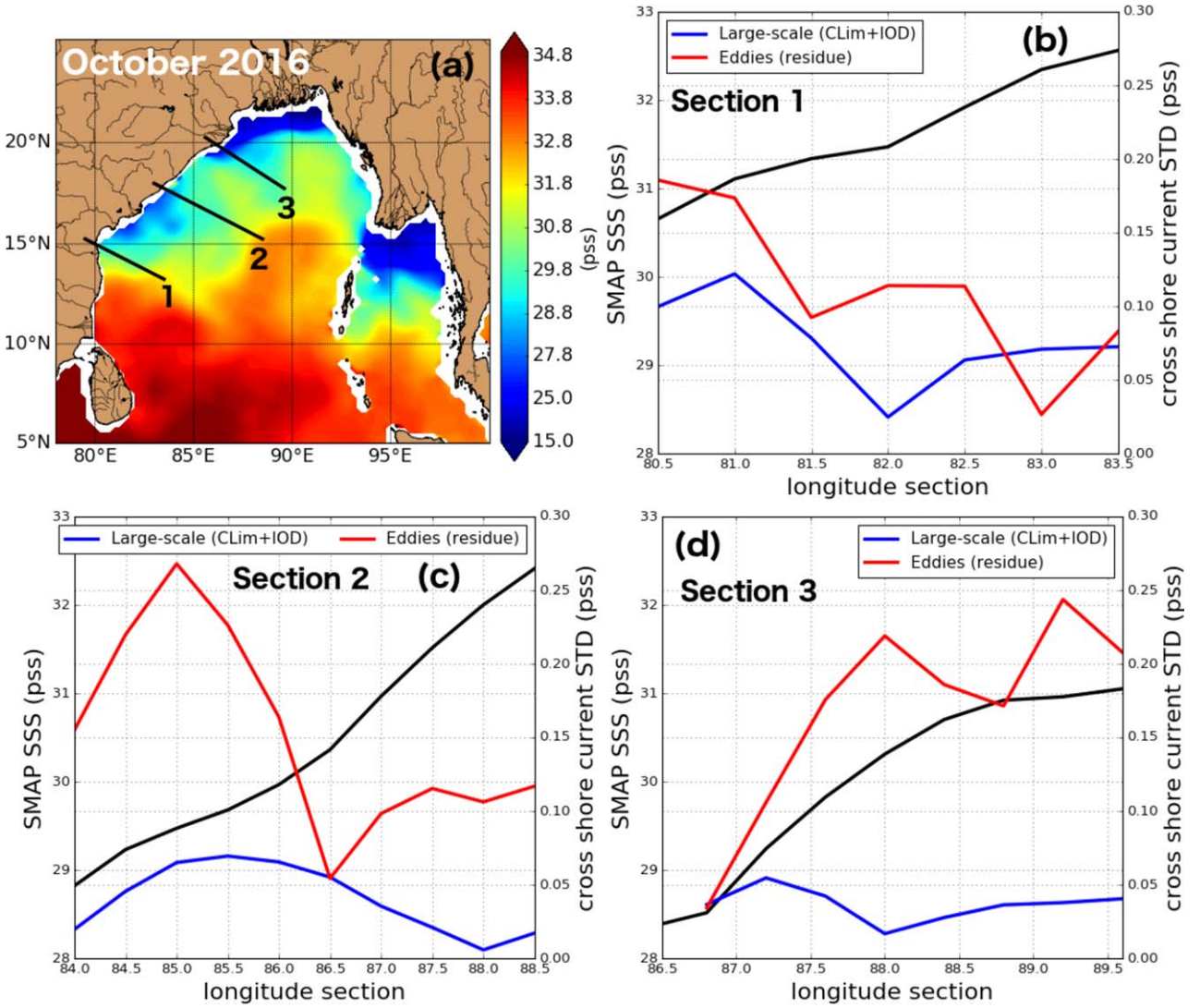


**Figure 12.** (a) October 2016 SMAP SSS. (b–d) Average SMAP SSS (black), large-scale (blue), and eddy-induced (red) cross-shore currents standard deviation along (b) section 1, (c) section 2, and (d) section 3 materialized by the black solid lines on plot Figure 12a. The large-scale currents are obtained by adding the mean seasonal cycle and anomalies with respect to the seasonal cycle associated with the IOD, obtained through a regression of the current fields to the normalized SON DMI (Dipole Mode Index). The eddy-induced currents are obtained as a residue, by subtracting the large-scale currents to the total altimetric currents observed. SLA has been detrended over the 1993–2016 period.

anomalies attributable to the IOD in October 2015 and 2016 (obtained through a linear regression to the normalized DMI, see section 2). Consistent with the model results from Akhil et al. (2016b), the 2015 positive IOD event is responsible for a large part of the large-scale negative SLA anomalies observed in October around the rim of the BoB (Figures 8a and 8c). This results in an anticyclonic circulation with particularly strong northward current anomalies along the eastern coast of India (Figure 8c), leading to an anomalously weak southward EICC and freshwater transport in fall relative to the seasonal climatology. The negative IOD event in 2016 also explains most of the positive SLA and current anomalies (Figures 8b and 8d), resulting in an anomalously strong southward EICC and freshwater transport. Anomalous maps similar to Figure 8 are shown in supplemental materials for September and November 2015 and 2016 (Figures 9 and 10), illustrating that similar but weaker anomalies were also present those months.

The results above clearly demonstrate the large-scale remote IOD influence on postmonsoon coastal freshening along the east coast of India. However, Figure 5 also reveals smaller-scale SSS features in regions of strong gradients, which were previously linked with mesoscale oceanic eddies (e.g., Babu et al., 1991; Hareesh Kumar et al., 2013; Murty et al., 1992). To relate these smaller-scale SSS features with mesoscale eddy variability,

Figures 8a and 8b display the SLA anomalies with respect to the mean seasonal cycle in October 2015 and 2016 (Figures 9 and 10 for September and November months, and Figure 11 for a zoom of SSS and currents). Many mesoscale eddies are clearly visible, and those coinciding with strong SSS gradients were reported by thick black arrows. For instance, a cyclonic eddy around 18°N carries the freshwater plume further south in September 2016 than in September 2015, when an anticyclonic eddy prevents the transport (Figures 5a, 5b, 9a, 9b, 11a, and 11b). A cyclonic and anticyclonic eddy pair induces an offshore meandering of the freshwater plume around 17°N, 86°E in October 2015 (Figures 5c, 8a, and 11c). In contrast, saltier water is transported from the interior BoB to the coast in association with another eddy pair, around 19°N in October 2016 (Figures 5d, 8b, and 11d). In November 2015, an eddy pair brings saltier interior BoB water to the coast near 19°N (Figures 5e, 10a, and 11e). These few examples illustrate that eddies tend to bring salty water to the coast and export freshwater offshore. This is supported by Figure 12, which shows the mean salinity and contributions of large-scale versus mesoscale eddy to cross-shore current variability along three sections perpendicular to the Indian coast. Eddies generally display larger cross-shore current variability than large-scale currents. They are hence important contributors to the offshore freshwater transport (i.e., they tend to increase SSS close to the coast and to increase it further away). Finally, it should be noted that the good correspondence between the completely independent altimeter surface currents and SMAP SSS (Figure 11) cannot be coincidental, and is a testimony of the ability of both data sets to capture fine-scale salinity structures in the BoB.

## 4. Concluding Remarks

In this study, we demonstrate the unprecedented capability of SMAP SSS to provide intraseasonal to interannual synoptic views of the sharp cross-shore SSS variations during the postmonsoon season in the BoB. SMAP SSS compares well with in situ data over the period of study with an overall correlation of 0.83 and RMSD of 0.49 pss. There is in particular no degradation of the SMAP performance within 40–200 km of the coast, where the SSS variability is particularly large, providing a favorable signal to noise ratio for monitoring SSS there. SMAP thus provides synoptic, intraseasonal to interannual monitoring of the "river in the sea," a capability not afforded by in situ data (Figure 1). SMAP SSS also presents an advantage over existing satellite SSS retrievals from SMOS, which excluded data from much of the northern BoB due to data quality issues, and Aquarius/SAC-D, which did not have sufficient resolution to resolve coastal signals (Akhil et al., 2016a).

SMAP satellite data are able to capture the GB freshwater plume carried by the southward-flowing postmonsoon EICC along the east coast of India, down to Sri Lanka, creating a narrow tongue of freshwater that hugs the east coast of India. In addition to capturing the seasonal variability of the BoB SSS signals, the short SMAP record along with ancillary data, such as altimetry, enable an illustration of some features of intraseasonal and interannual SSS variability. On interannual timescales, we were able to confirm the modulation of the EICC/GB plume southward extent by the IOD suggested by Akhil et al. (2016b). There was a positive IOD event in fall 2015 and a negative one in fall 2016. This led to a stronger southward EICC in 2016, especially south of 14°N. The GB freshwater plume hence extended further south in 2016, all the way down to the coast of Sri Lanka, while it did not flow past 14°N in 2015. On intraseasonal timescales, our results reveal a clear stirring of the SSS field by BoB mesoscale eddies associated with EICC recirculations that export freshwater from the coast to the BoB interior, as suggested by Hareesh Kumar et al. (2013) from in situ data and Benshila et al. (2014) from modeling.

Due to strong salinity stratification, the BoB is less productive than the neighboring Arabian Sea (Prasanna Kumar et al., 2002). The salinity stratification could also contribute to climatologically strong rainfall during the southwest monsoon (Shenoi et al., 2002) and to hurricane intensification (Neetu et al., 2012; Sengupta et al., 2008). Despite this potential importance of salinity, available in situ salinity measurements are inadequate for a comprehensive study of salinity variability and the associated processes in the BoB. SMAP, with its 8 day temporal repeat, opens a new avenue to improve the understanding of BoB salinity balance, the contribution of horizontal salinity gradients to the EICC, the offshore freshwater transport by eddies, and the exchanges of freshwater between the BoB and saltier Arabian Sea.

**Acknowledgments**
The research described in this paper was carried out at the Jet Propulsion Laboratory, California Institute of Technology, under a contract with NASA. It is in part supported by the NASA Postdoctoral Program administered by the Universities Space Research Association (USRA). J.V. and M.L. are supported by Institut de Recherche pour le Développement (IRD), Centre National de Recherche Spatiale (CNES), and the LEFE-EC2CO program (AO2016-985784 proposal). A.V.S.C. is supported by Institut de Recherche pour le Developpement (IRD). Bottle salinity data were collected under support from Ministry of Earth Sciences (Government of India, odis.incois.gov.in). Data used in this paper are available at the following data centers: NASA Physical Oceanography Distributed Active Archive Center (PO.DAAC) for SMAP SSS data (https://podaac.jpl.nasa.gov/dataset/SMAP_JPL_L3_SSS_CAP_8DAY-RUNNINGMEAN_V3; the NOAA NODC World Ocean Database (WOD) select for in situ salinity data (https://www.nodc.noaa.gov/cgi-bin/OC5/SELECT/dbsearch.pl); Copernicus Marine and Environment Monitoring Service (CMEMS) for the AVISO SLA data (http://www.marine.copernicus.eu); Ssalto/Duacs and AVISO for the ocean currents data (http://www.aviso.altimetry.fr/duacs/); and JAMSTEC for the DMI index (http://www.jamstec.go.jp/frcgc/research/d1/iod/DATA/dmi.monthly.txt). The bucket samples collected by the National Institute of Oceanography (Goa, India) are available in supporting information Table S1.

## References

Akhil, V. P., Durand, F., Lengaigne, M., Vialard, J., Keethi, M. G., Gopalakrishna, V. V., . . . de Boyer Montégut, C. (2014). A modeling study of the processes of surface salinity seasonal cycle in the Bay of Bengal. *Journal of Geophysical Research: Oceans*, *116*, 3926–3947. https://doi.org/10.1002/2013JC009632

Akhil, V. P., Lengaigne, M., Durand, F., Vialard, J., Chaitanya, A. V. S., Keerthi, M. G., . . . de Boyer Montégut, C. (2016a). Assessment of seasonal and year-to-year surface salinity signals retrieved from SMOS and Aquarius missions in the Bay of Bengal. *International Journal of Remote Sensing*, *37*(5), 1089–1114. https://doi.org/10.1080/01431161.2016.1145362

Akhil, V. P., Lengaigne, M., Vialard, J., Durand, F., Keerthi, M. G., Chaitanya, A. V. S., . . . de Boyer Montégut, C. (2016b). A modeling study of processes controlling the Bay of Bengal sea surface salinity interannual variability. *Journal of Geophysical Research: Oceans*, *121*, 8471–8495. https://doi.org/10.1002/2016JC011662

Aquarius User Guide (2015). Retrieved from ftp://podaac-ftp.jpl.nasa.gov/allData/aquarius/docs/v4/AQ-010-UG-0008_AquariusUserGuide_DatasetV4.0.pdf

Babu, M. T., Prasanna Kumar, S., & Rao, D. P. (1991). A subsurface cyclonic eddy in the Bay of Bengal. *Journal of Marine Research*, *49*(3), 403–410. https://doi.org/10.1357/002224091784995846

Benshila, R., Durand, F., Masson, S., Bourdallé-Badie, R., de Boyer Montégut, C., Papa, F., & Madec, G. (2014). The upper Bay of Bengal salinity structure in a high-resolution model. *Ocean Modelling*, *74*, 36–52. https://doi.org/10.1016/j.ocemod.2013.12.001

Boutin, J., Chao, Y., Asher, W. E., Delcroix, T., Drucker, R., Drushka, K., . . . Ward, B. (2015). Satellite and in situ salinity: Understanding near-surface stratification and subfootprint variability. *Bulletin of the American Meteorological Society*, *97*, 1391–1407. https://doi.org/10.1175/BAMS-D-15-00032.1

Boutin, J., Martin, N., Yin, X., Font, J., Reul, N., & Spurgeon, P. (2012). First assessment of SMOS data over open ocean: Part II—Sea surface salinity. *IEEE Transactions on Geoscience and Remote Sensing*, *50*, 1662–1675. https://doi.org/10.1109/TGRS.2012.2184546

Boyer, T. P., Antonov, J. I., Baranova, O. K., Coleman, C., Garcia, H. E., Grodsky, A., . . . Zweng, M. M. (2013). In S. Levitus and A. Mishonov (Eds.), *World ocean database 2013, NOAA Atlas NESDIS 72* (209 p.). Silver Spring, MD: National Oceanographic Data Center, Ocean Climate Laboratory. http://doi.org/10.7289/V5NZ85MT

Chaitanya, A. V. S., Durand, F., Mathew, S., Gopalakrishna, V. V., Papa, F., Lengaigne, M., . . . Venkatesan, R. (2015). Observed year-to-year sea surface salinity variability in the Bay of Bengal during the period 2009–2014. *Ocean Dynamics*, *65*, 173–186. https://doi.org/10.1007/s10236-014-0802-x

Chaitanya, A. V. S., Lengaigne, M., Vialard, J., Gopalakrishna, V. V., Durand, F., KranthiKumar, C., . . . Ravichandran, M. (2014). Salinity measurements collected by fishermen reveal a "river in the sea" flowing along the Eastern Coast of India. *Bulletin of the American Meteorological Society*, *95*, 1897–1908. https://doi.org/10.1175/BAMS-D-12-00243.1

Cione, J. J., & Uhlhorn, E. W. (2003). Sea surface temperature variability in hurricanes: Implications with respect to intensity change. *Monthly Weather Review*, *131*, 1783–1796. https://doi.org/10.1175//2562.1

Dai, A., & Trenberth, K. E. (2002). Estimates of freshwater discharge from continents: Latitudinal and seasonal variations. *Journal of Hydrometeorology*, *3*(6), 660–687. https://doi.org/10.1175/1525-7541(2002)003<0660:EOFDFC>2.0.CO;2

Durand, F., Shankar, D., Birol, F., & Shenoi, S. S. C. (2008). Estimating boundary currents from satellite altimetry: A case study for the east coast of India. *Journal of Oceanography*, *64*(6), 831–845. https://doi.org/10.1007/s10872-008-0069-2

Durand, F., Shankar, D., Birol, F., & Shenoi, S. S. C. (2009). Spatio temporal structure of the East India Coastal Current from satellite altimetry. *Journal of Geophysical Research*, *114*, C02013. https://doi.org/10.1029/2008JC004807

Fournier, S., Reager, J. T., Lee, T., Vazquez-Cuervo, J., David, C. H., & Gierach, M. M. (2016). SMAP observes flooding from land to sea: The Texas event of 2015. *Geophysical Research Letters*, *43*, 10338–10346. https://doi.org/10.1002/2016GL070821

Hareesh Kumar, P. V., Mathew, B., Kumar, M. R. R., Rao, A. R., Jagadeesh, P. S. V., Radhakrishnan, K. G., & Shyni, T. N. (2013). Thermohaline front' off the east coast of India and its generating mechanism. *Ocean Dynamics*, *63*(11–12), 1175–1180. https://doi.org/10.1007/s10236-013-0652-y

Jensen, T. G. (2007). Wind-driven response of the northern Indian Ocean to climate extremes. *Journal of Climate*, *20*, 2978–2993. https://doi.org/10.1175/JCLI4150.1

Lagerloef, G., Colomb, F. R., Le Vine, D., Wentz, F., Yueh, S., Ruf, C., . . . Swift, C. (2008). The aquarius/SAC-D mission: Designed to meet the salinity remote sensing challenge. *Oceanography*, *21*(1), 68–81. https://doi.org/10.5670/oceanog.2008.68

McCreary, J. P., Han, W., Shankar, D., & Shetye, S. R. (1996). Dynamics of the East India Coastal current: 2. Numerical solutions. *Journal of Geophysical Research*, *101*, 13993–14010. https://doi.org/10.1029/96JC00560

Mecklenburg, S., Drusch, M., Kerr, Y. H., Font, J., Martin-Neira, M., Delwart, S., . . . Crapolicchio, R. (2012). ESA's soil moisture and ocean salinity mission: Mission performance and operations. *IEEE Transactions on Geoscience and Remote Sensing*, *50*(5, Part 1), 1354–1366. https://doi.org/10.1109/TGRS.2012.2187666

Murty, V. S. N., Sarma, Y. V. B., Rao, D. P., & Murty, C. S. (1992). Water characteristics, mixing and circulation in the Bay of Bengal during southwest monsoon. *Journal of Marine Research*, *50*(2), 207–228. https://doi.org/10.1357/002224092784797700

Neetu, S., Lengaigne, M., Vincent, E. M., Vialard, J., Madec, G., Samson, G., . . . Durand, F. (2012). Influence of upper-ocean stratification on tropical cyclones-induced surface cooling in the Bay of Bengal. *Journal of Geophysical Research*, *117*, C12020. https://doi.org/10.1029/2012JC008433

Papa, F., Bala, S. K., Pandey, R. K., Durand, F., Gopalakrishna, V. V., Rahman, A., & Rossow, W. B. (2012). Ganga-Brahmaputra river discharge from Jason-2 radar altimetry: An update to the long-term satellite-derived estimates of continental freshwater forcing flux into the Bay of Bengal. *Journal of Geophysical Research*, *117*, C11021. https://doi.org/10.1029/2012JC008158

Prasanna Kumar, S., Muraleedharan, P. M., Prasad, T. G., Gauns, M., Ramaiah, N., Souza, S. N., . . . Madhupratap, M. (2002). Why is the Bay of Bengal less productive during summer monsoon compared to the Arabian Sea? *Geophysical Research Letters*, *29*(24), 2235. https://doi.org/10.1029/2002GL016013

Rao, R. R., & Sivakumar, R. (2003). Seasonal variability of the salt budget of the mixed layer and near-surface layer salinity structure of the tropical Indian Ocean from a new global ocean salinity climatology. *Journal of Geophysical Research*, *108*(C1), 3009. https://doi.org/10.1029/2001JC000907

Reul, N., Fournier, S., Boutin, J., Hernandez, O., Maes, C., Chapron, B., . . . Delwart, S. (2013). Sea surface salinity observations from space with the SMOS satellite: A new means to monitor the marine branch of the water cycle. *Surveys in Geophysics*, *35*, 681–722. https://doi.org/10.1007/s10712-013-9244-0

Saji, N. H., Goswami, B. N., Vinayachandran, P. N., & Yamagata, T. (1999). A dipole mode in the tropical Indian Ocean. *Nature*, *401*(6751), 360–363. https://doi.org/10.1038/43854

Sengupta, D., Bharath Raj, G. N., Ravichandran, M., Sree Lekha, J., & Papa, F. (2016). Near-surface salinity and stratification in the north Bay of Bengal from moored observations. *Geophysical Research Letters*, *43*, 4448–4456. https://doi.org/10.1002/2016GL068339

Sengupta, D., Goddalehundi, B. R., & Anitha, D. S. (2008). Cyclone-induced mixing does not cool SST in the post-monsoon North Bay of Bengal. *Atmospheric Science Letters*, *9*(1), 1–6. https://doi.org/10.1002/asl.162

Shankar, D. (1998). *Low-frequency variability of sea level along the coast of India*, (PhD thesis, 207 p.). Goa, India: Goa University. Retrieved from http://drs.nio.org/drs/handle/2264/24

Shenoi, S. S. C., Shankar, D., & Shetye, S. R. (2002). Difference in heat budgets of the near-surface Arabian Sea and Bay of Bengal: Implications for the summer monsoon. *Journal of Geophysical Research*, *107*(C6), 3052. https://doi.org/10.1029/2000JC000679

Shetye, S. R., Gouveia, A. D., Shankar, D., Michael, G. S., & Nampoothiri, G. (1996). Hydrography and circulation of the western Bay of Bengal during the Northeast Monsoon. *Journal of Geophysical Research*, *101*, 14011–14025. https://doi.org/10.1029/95JC03307

Subrahmanyam, B., Grunseich, G., & Nyadjro, E. S. (2013). Preliminary SMOS salinity measurements and validation in the Indian Ocean. *IEEE Transcations on Geoscience and Remote Sensing*, *51*, 19–27. https://doi.org/10.1109/TGRS.2012.2199122

Subrahmanyam, B., Murty, V. S. N., & Heffner, D. M. (2011). Sea surface salinity variability in the tropical Indian Ocean. *Remote Sensing of Environment*, *115*(3), 944–956. https://doi.org/10.1016/j.rse.2010.12.004

Thadathil, P., Suresh, I., Gautham, S., Prasanna Kumar, S., Lengaigne, M., Akshay, H., . . . Somayajulu, Y. K. (2016). Intraseasonal to interannual variability of surface layer temperature inversion in the Bay of Bengal: Main characteristics and related mechanisms. *Journal of Geophysical Research: Oceans*, *121*, 5682–5696. https://doi.org/10.1002/2016JC011674

Thompson, P. R., Piecuch, C. G., Merrifield, M. A., McCreary, J. P., & Firing, E. (2016). Forcing of recent decadal variability in the Equatorial and North Indian Ocean. *Journal of Geophysical Research: Oceans*, *121*, 6762–6778. https://doi.org/10.1002/2016JC012132

Vialard, J., & Delecluse, P. (1998). An OGCM study for the TOGA decade. Part I: Role of salinity in the physics of the western Pacific fresh pool. *Journal of Physical Oceanography*, *28*, 1071–1088. https://doi.org/10.1175/1520-0485(1998)028<1071:AOSFTT>2.0.CO;2

Vinaychandran, P., Murty, V. S. N., & Ramesh Babu, V. (2002). Observations of barrier layer formation in the Bay of Bengal during summer monsoon. *Journal of Geophysical Research*, *107*(C12), 8018. https://doi.org/10.1029/2001JC000831

Wijesekera, H. W. *et al*. (2016). ASIRI: An ocean-atmosphere initiative for Bay of Bengal. *Bulletin of the American Meteorological Society*, *97*(10), 1859–1884. https://doi.org/10.1175/BAMS-D-14-00197.1

Yu, L., O'Brien, J. J., & Yang, J. (1991). On the remote forcing of the circulation in the Bay of Bengal. *Journal of Geophysical Research*, *96*, 20449–20454. https://doi.org/10.1029/91JC02424

Yueh, S. H., Tang, W., Fore, A. G., Neumann, G., Hayashi, A., Freedman, A., . . . Lagerloef, G. S. (2013). L-band passive and active microwave geophysical model functions of ocean surface winds and applications to Aquarius retrieval. *IEEE Transactions on Geoscience and Remote Sensing*, *51*(9), 4619–4632. https://doi.org/10.1109/TGRS.2013.2266915

Yueh, S. H., Tang, W., Fore, A., Hayashi, A., Song, Y. T., & Lagerloef, G. (2014). Aquarius geophysical model function and combined active passive algorithm for ocean surface salinity and wind retrieval. *Journal of Geophysical Research: Oceans*, *119*, 5360–5379. https://doi.org/10.1002/2014JC009